Progress In Electromagnetics Research C, Vol. 137, 65–79, 2023

Study of a Double-Layer Passive Magnetic Shielding System for Electric Vehicle WPT

Xueyi Zhang[1], Liquan Ren[1], Pengsheng Kong[3], Xinbo Xiong[1], and Zhongqi Li[1, 2, 3, *]

Abstract—In the wireless power transfer (WPT) system of electric vehicles, the magnetic shielding performance often comes at the expense of the transmission efficiency. How to maintain high transmission efficiency while reducing magnetic leakage is a challenge. For this reason, this paper proposes a double-layer passive magnetic shielding coil structure for an electric vehicle WPT system. First, a leakage optimization method is given, and the optimal parameters for each shielding coil are obtained with this method. Second, according to the obtained coil parameters, a WPT system with magnetic shielding for electric vehicles is developed. The correctness of the proposed structure and method is verified by simulation and experiment. Finally, when the system output is 4 kW, the proposed shielding structure not only reduces the maximum leakage field in the target area by 54.64%, but also has a transmission efficiency of 94.8%.

1. INTRODUCTION

In recent years, magnetic coupling resonant WPT technology has received much attention from scholars and industry [1–4]. A WPT system has a high level of security, high space availability, nonabrasiveness, etc. It has been widely used in implantable medical devices [5], rail transportation [6], electric vehicles [7–10], etc. The development of this technology breaks the limitations of traditional wired electrical energy transmission. However, at the same time, the system generates leakage magnetic fields that can be harmful to humans [11, 12].

Magnetic shielding measures to effectively reduce the leakage of magnetic fields from the system can be generally divided into proactive and reactive shielding. Reactive shielding uses metal plates and magnetic cores to suppress perpendicular leakage, which exploits the eddy current effect of the metal. This is a simple but costly method, and the eddy current effect also causes heat loss resulting in reduced transmission efficiency [13–15].

Proactive shielding can be further divided into active and passive shielding, depending on the form of the excitation. In active shielding, a shielding coil is connected in series with the main coil, or an additional excitation is applied to the shielding coil to obtain a counteracting magnetic field in the opposite direction to that of the main coil. Cruciani and Campi of the University of L'Aquila [16] and Meng and Zhang of the University of Chinese Academy of Sciences [17] used separate active shielding coils placed horizontally and vertically on both sides of the main coil to effectively reduce the magnetic field leakage on both sides of the main coil. However, the reverse flux directly weakened the main flux and thus directly affected the transmission efficiency. Thus, Zhou's team at Chongqing University placed anti-series shielding coils above a metal shield to reduce the effect on the main magnetic flux [18]. In addition, Xu of Harbin Institute of Technology and other scholars placed an anti-series shielding coil

Received 21 April 2023, Accepted 17 August 2023, Scheduled 29 August 2023

* Corresponding author: Zhongqi Li (my3eee@126.com).

[1] College of Electrical and Information Engineering, Hunan University of Technology, Zhuzhou 412007, China. [2] College of Electrical and Information Engineering, Hunan University, Changsha 412008, China. [3] College of Railway Transportation, Hunan University of Technology, Zhuzhou 412007, China.

below the receiving coil and tilted it to a certain angle. Therefore, the shielding coil flux formed a certain angle with the main flux, thus further reducing the influence on the main flux [19]. However, the effect of active shielding on the main magnetic flux was still very noticeable. Passive shielding uses electromagnetic induction to produce an excitation and counteracts the magnetic field by adjusting the matching capacitance. This type of shielding does not consume additional power, and the reverse flux is at an angle to the main flux; thus, this configuration has a high transmission efficiency while obtaining good shielding [20]. Lee and Kim of the Korea Institute of Science and Technology and other scholars [21] proposed a novel hybrid loop array structure. The array structure combines a shielding coil to reduce the strength of the magnetic field leakage and an amplifying coil to enhance the magnetic field strength between the coupling coils. In addition, the Institute's Kim and Park [22] placed shielding coils vertically farther on either side of the main coil to reduce the magnetic field leakage. However, the shielding effect was not obvious; additional shielding coils were then placed closer to the main coil to improve the shielding effect [23], and the reduction in the transmission efficiency was not obvious. However, the additional shielding coils further increase the size of the system.

With regard to the above shielding methods, we can summarize some of the characteristics, as shown in Table 1 below.

Table 1. Classification table of shielding methods.

Shielding methods	Shielding materials	Advantages	Disadvantages
Passive shielding	Ferromagnetic metals	Good magnetic field modulation	High costs
	Non-ferromagnetic metals	Good magnetic shielding	High eddy current losses
Active shielding	Source coils	Flexible space location	Influence on main coil coupling
	Without source coils	Good controllability	Parameter design difficulties

In this paper, a double-layer passive magnetic shielding coil structure for electric vehicles is proposed. This structure uses the leakage magnetic field of the WPT coil to provide excitation for the shielding coil, thereby generating a large range of reverse flux on both sides of the vehicle. Because the mutual inductance between the shielding coil and the transceiver coil is small, the shielding coil acts as a shield while barely affecting the transmission efficiency of the WPT system. In addition, the coil parameters are optimized based on the theory presented below; finally, an experimental platform is built to verify the reliability of the method.

2. COIL MAGNETIC FIELD CALCULATION

To calculate the magnetic field distribution in space, this section focuses on introducing a magnetic vector potential-based calculation of the magnetic field of a rectangular coil [24]. Figure 1 shows the spatial location of the rectangular coil, where a_1 and a_2 are the half-length and half-width of the coil; O is the midpoint of the coil; z_0 is the height of the coil; and I is the current flowing through the coil.

For a current carrying conductor with current density $\vec{J}$ in air, the magnetic vector potential generated at any point $P(x, y, z)$ is as follows:

$$\vec{A}(x, y, z) = \frac{\mu_0}{4\pi} \int_v \frac{\vec{J}(x', y', z')\, dv'}{\vec{R}} \tag{1}$$

where v is the current distribution of the conductor, and $\vec{R}$ is the distance between any point $P(x, y, z)$ and the point source $P(x', y', z')$.

The incident flux density is known to be related to the magnetic vector potential by the following equation:

$$\vec{B} = \nabla \times \vec{A} \tag{2}$$

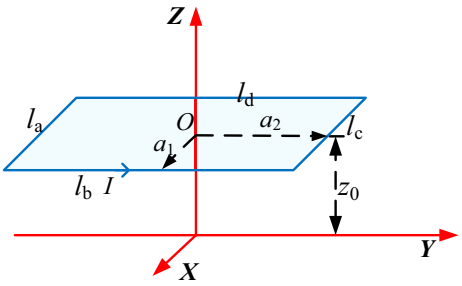

Figure 1. Schematic representation of the spatial location of the rectangular coil.

The flux density is obtained as follows:

$$\dot{B}_x = \frac{1}{4\pi^2}\int_{-\infty}^{\infty}\int_{-\infty}^{\infty}\frac{j2\mu_0 I\sin(\xi a_1)\sin(\eta a_2)}{\eta}\cdot e^{j(x\xi+y\eta)}d\xi d\eta \tag{3}$$

$$\dot{B}_y = \frac{1}{4\pi^2}\int_{-\infty}^{\infty}\int_{-\infty}^{\infty}\frac{j2\mu_0 I\sin(\xi a_2)\sin(\eta a_1)}{\xi}\cdot e^{j(x\xi+y\eta)}d\xi d\eta \tag{4}$$

$$\dot{B}_z = \frac{1}{4\pi^2}\int_{-\infty}^{\infty}\int_{-\infty}^{\infty}\frac{-2\sqrt{\xi^2+\eta^2}\mu_0 I\sin(\xi a_1)\sin(\eta a_2)}{\xi\eta}\cdot e^{j(x\xi+y\eta)}d\xi d\eta \tag{5}$$

$$\dot{B} = \sqrt{\left|\dot{B}_x\right|^2+\left|\dot{B}_y\right|^2+\left|\dot{B}_z\right|^2} \tag{6}$$

The magnetic field theory presented in this section provides the theoretical basis for the leakage optimization below.

3. DOUBLE-LAYER PASSIVE MAGNETIC SHIELDING STRUCTURE AND ITS PRINCIPLE

To reduce the magnetic leakage on both sides of the door when charging a car, this section first proposes a double-layer passive magnetic shielding coil structure. By analyzing the equivalent circuit model of this structure, it is found that this structure has a good magnetic shielding effect from the physical and mathematical points of view.

3.1. Double-Layer Passive Magnetic Shielding Structure

The structure of the proposed double-layer passive magnetic shielding coils for electric vehicles is shown in Figure 2.

In Figure 2, T_x is the transmitting coil; R_x is the receiving coil; and Sh_1, Sh_2, Sh_3, and Sh_4 are passive shielding coils. Transmitting coil T_x is at the same height as shielding coils Sh_1 and Sh_3, and receiving coil R_x is at the same height as the shielding coils Sh_2 and Sh_4. The transmission distance between the transmitting and receiving coils is 15 cm. The width of an electric vehicle is generally 160 cm, so the magnetic leakage observation surfaces are located 80 cm from the midpoint of the receiving coil.

According to the coil structure in Figure 2, the equivalent circuit diagram of the system is obtained as shown in Figure 3, where L_i and R_i are the self-inductance and internal resistance of each coil ($i = 1, 2, 3, 4, 5, 6$); C_1 is the resonant capacitance of the transmitting coil; and C_2 is the resonant capacitance of the receiving coil. C_3, C_4, C_5, and C_6 are the matching capacitances of the shielding coil, which are used to control the phase and current amplitude of the shielding current. M_{ij} is the mutual inductance between coils i and j ($i, j = 1, 2, 3, 4, 5, 6$); V_S is the excitation of the transmitting coil; and R_L is the load. Since the two sides are far apart, only the mutual inductance between the shielding coils on the same side is considered in this paper.

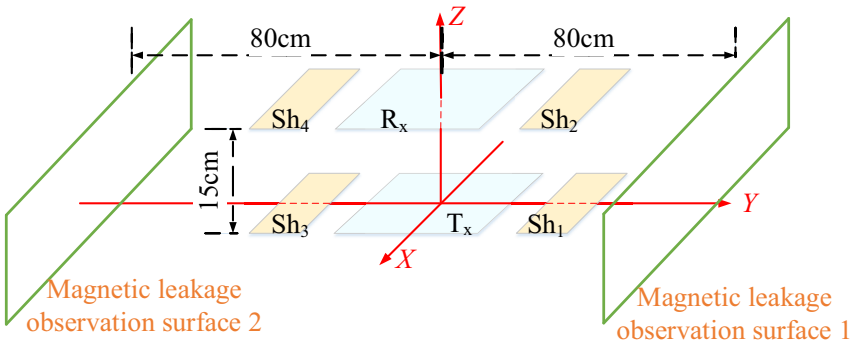

Figure 2. Double-layer passive magnetic shielding coils spatial structure diagram.

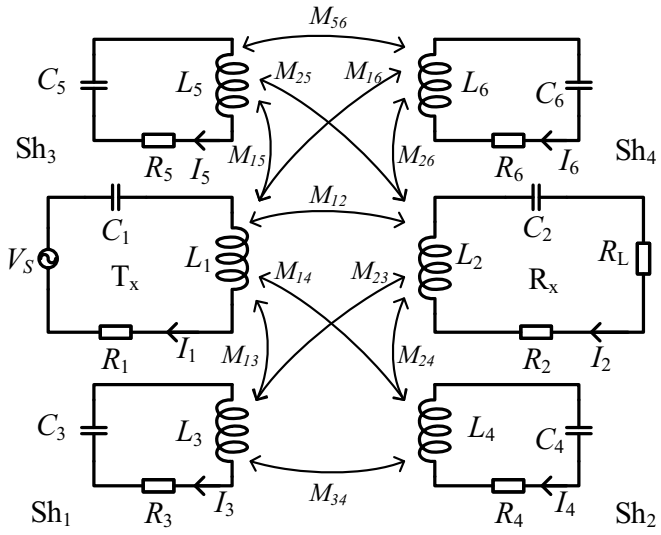

Figure 3. System equivalent circuit diagram.

A matrix of the Kirchhoff voltage equations can be derived from the circuit diagram in Figure 3.

$$\begin{bmatrix} \dot{Z}_1 & j\omega M_{12} & j\omega M_{13} & j\omega M_{14} & j\omega M_{15} & j\omega M_{16} \\ j\omega M_{21} & \dot{Z}_2 & j\omega M_{23} & j\omega M_{24} & j\omega M_{25} & j\omega M_{26} \\ j\omega M_{31} & j\omega M_{32} & \dot{Z}_3 & j\omega M_{34} & 0 & 0 \\ j\omega M_{41} & j\omega M_{42} & j\omega M_{43} & \dot{Z}_4 & 0 & 0 \\ j\omega M_{51} & j\omega M_{52} & 0 & 0 & \dot{Z}_5 & j\omega M_{56} \\ j\omega M_{61} & j\omega M_{62} & 0 & 0 & j\omega M_{65} & \dot{Z}_6 \end{bmatrix} \begin{bmatrix} \dot{I}_1 \\ \dot{I}_2 \\ \dot{I}_3 \\ \dot{I}_4 \\ \dot{I}_5 \\ \dot{I}_6 \end{bmatrix} = \begin{bmatrix} \dot{V}_S \\ 0 \\ 0 \\ 0 \\ 0 \\ 0 \end{bmatrix} \tag{7}$$

From the above matrix, the current of each coil is obtained, where $Z_1 = R_1$, $Z_2 = R_2 + R_{\mathrm{L}}$, $Z_3 = R_3 + j\omega L_3 - 1/j\omega C_3$, $Z_4 = R_4 + j\omega L_4 - 1/j\omega C_4$, $Z_5 = R_5 + j\omega L_5 - 1/j\omega C_5$, and $Z_6 = R_6 + j\omega L_6 - 1/j\omega C_6$.

3.2. Double-Layer Passive Magnetic Shielding Principle

The shielding principle of this system is shown in Figure 4. The double-layer shielding coils are positioned parallel to the transmitting and receiving coils, and when the shielding coil receives the leakage flux from the transmitting and receiving coils, an induced voltage $\dot{V}_{\mathrm{ind}}$ is generated on the shielding coil

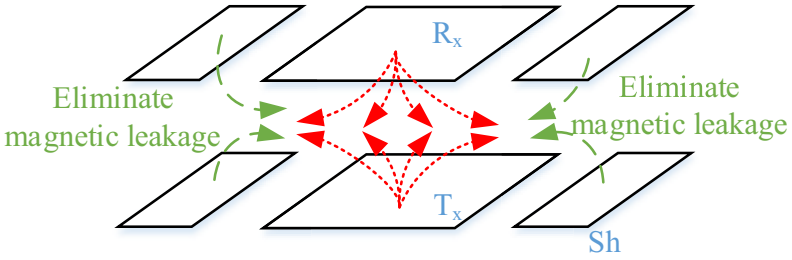

Figure 4. Shielding structure schematic.

with the following expression:

$$\dot{V}_{\text{ind}} = \int \dot{E} \cdot dl = -\frac{d\phi}{dt} = -\frac{d\dot{B} \cdot S}{dt} \tag{8}$$

where B is the time-varying leakage magnetic field generated by the transmitting and receiving coils, which can be expressed as:

$$\dot{B} = \dot{B}_0 \cdot e^{j\omega t} = \dot{B}_0 \cos\omega t + j\,\dot{B}_0 \sin\omega t \tag{9}$$

Thus, Equation (21) can be expressed as follows:

$$\dot{V}_{\text{ind}} = -j\omega \dot{B}_0 \cdot e^{j\omega t} S \tag{10}$$

The shielding coil impedance $Z_{\text{Sh}} = R_{\text{Sh}} + j\omega L_{\text{Sh}} - 1/j\omega C_{\text{Sh}}$, and the coil inner group R_{Sh} is negligible. Then the current in the shielding coil can be expressed as:

$$\dot{I}_{\text{Sh}} = -\frac{j\omega \dot{B}_0 \cdot e^{j\omega t} S}{j\left(\omega L_5 - \dfrac{1}{\omega C_5}\right)} \tag{11}$$

From this, the magnetic leakage elimination generated by the shielding coil can be expressed according to the Biot-Savart law as:

$$\dot{B}_{\text{Sh}} = -\dot{B} \cdot \frac{\mu_0 j\omega S}{4\pi j\left(\omega L_{\text{Sh}} - \dfrac{1}{\omega C_{\text{Sh}}}\right)} \int_{c'} \frac{\vec{d_l} \times \vec{R}}{R^3} \tag{12}$$

It is easy to see that when $\omega L_{\text{Sh}} > 1/\omega C_{\text{Sh}}$ that is, when the matching capacitance of the shielding coil is less than the resonant capacitance, $\dot{B}_{\text{Sh}}$ and $\dot{B}$ are reversed, and the coil can have a shielding effect.

4. LEAKAGE OPTIMIZATION

In this section, the coil parameters for the double-layer passive magnetic shielding system are optimized by means of the magnetic field calculation formula for rectangular coils. When the coil parameters are optimal, the maximum magnetic leakage point on the leakage observation surface has the minimum magnetic leakage. The flow of coil optimization is shown in Figure 5 below. The specific optimization steps are as follows:

(1) Parameter setting and initialization: The vertical transmission distance between the transmitting and receiving coils is set to 15 cm. Both the transmitter and receiver coils have an inner edge length and width of 48 cm and a turn count of 15 turns, with parameters that are sized to fit into the vehicle chassis. Shielding coils Sh_1 and Sh_3 are at the same horizontal height as transmitting coil T_x. Shielding coils Sh_2 and Sh_4 are at the same horizontal height as receiving coil R_x. The conductor is a copper wire with a cross-sectional diameter of 3.43 mm, and the transmission power is set at 4 kW.

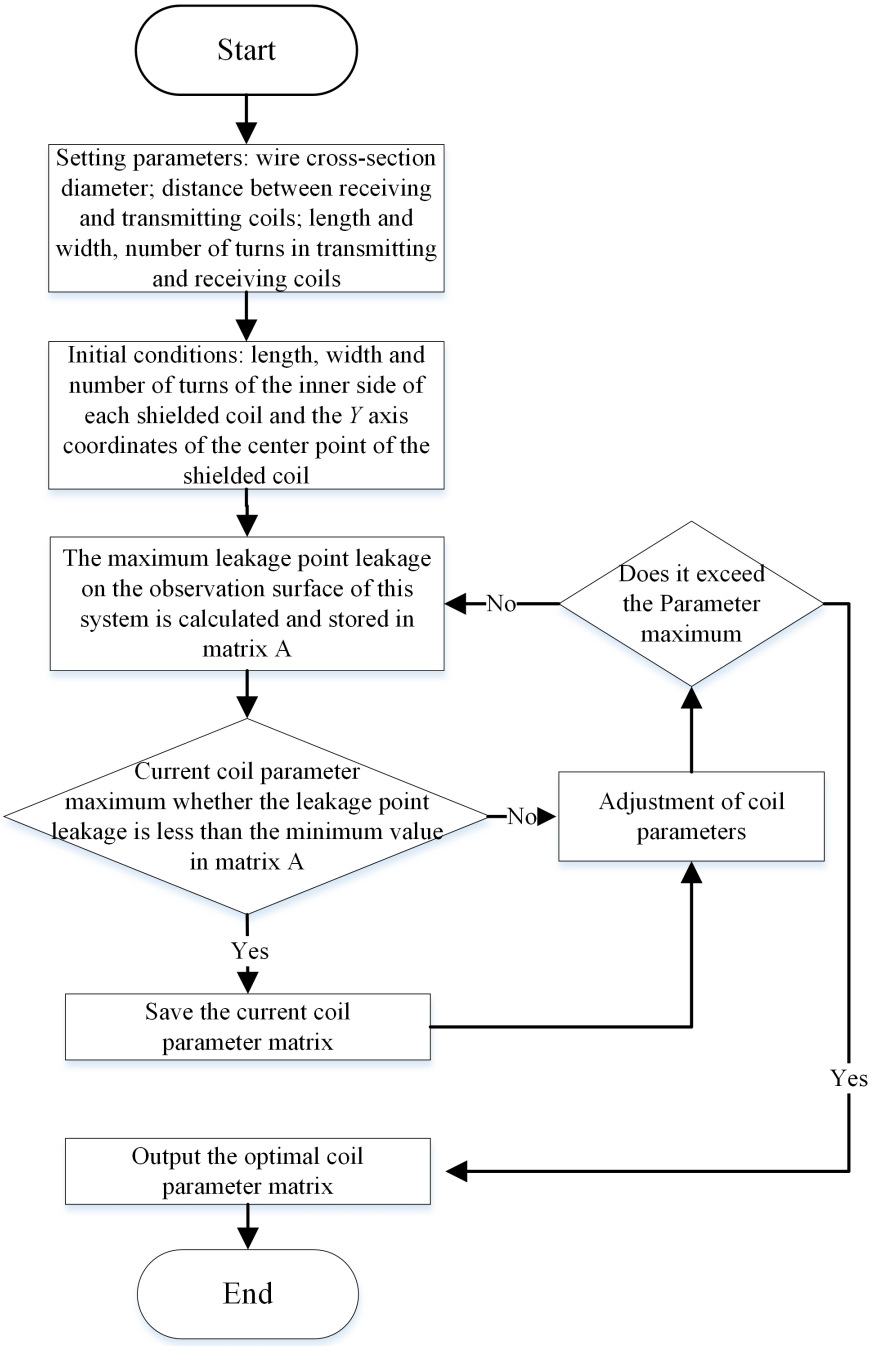

Figure 5. Coil optimization flowchart.

(2) Constraints setting: The constraints are set based on the actual situation. The Y-axis coordinate of the center point of the shielding coil is set to 40–50 cm, the inner length of the shielding coil set to 12–22 cm, the inner width set to 45–55 cm, and the number of turns set to 3–8 turns. The step for the number of turns is 1 turn, and the steps for the inner edge length and width and Y-axis coordinate are all 1 cm.

(3) Magnetic induction strength B calculation: The calculation is performed according to the formula for calculating the observation surface magnetic leakage. The leakage value at the maximum magnetic leakage point under the set coil parameters is stored in matrix A.

(4) Conditional judgment: Whether the leakage at the maximum magnetic leakage point of the observation surface under the present coil parameters is less than the minimum value in matrix A is judged. If this condition is satisfied, then the current coil parameters are saved. If not, then the coil parameters continue to be adjusted for calculation until all the parameters are run.

(5) Output of the optimal matrix parameters: The coil parameters with the smallest maximum magnetic leakage on the observation surface are output. The final coil parameters are as follows: the shielding coil center point Y-axis coordinate is 45 cm. Shielding coils Sh_1 and Sh_3 have an inner length of 50 cm, an inner width of 20 cm, and a number of turns of 5. Shielding coils Sh_2 and Sh_4 have an inner length of 50 cm, an inner width of 17 cm, and a number of turns of 4.

5. EXPERIMENTAL VERIFICATION

In this section, a double-layer shielding system for WPT of electric vehicles is built. The leakage B at the maximum leakage point on the target surface of the system and its transmission efficiency η are obtained through three methods: theoretical calculation, Ansys Maxwell electromagnetic simulation, and experiments.

5.1. Detailed Parameters of the Experimental Setup

The framework of the experimental system is shown in Figure 6 below.

In Figure 6, the DC source is inverted by the inverter module into a high-frequency AC, and the energy is transmitted by the transmitter coil to the receiver coil. Finally, the rectifier module converts the AC power into DC power for the load. The inverter module and rectifier module are both single-phase full-bridge circuits and use SiC power devices. Their model number is C3M0075120D, and the maximum current resistance is 30 A.

Based on the obtained parameters, a set of new coil physical models was developed. All coils are wound with Leeds wire to reduce the internal resistance, and the Leeds wire specifications are ϕ0.1 mm $\times$ 600 strands, with a maximum current of 23.5 A. The physical coil consists of a transmitting coil, a receiving coil, and four shielding coils, as shown in Figure 7. In addition, a WT5000 power analyzer is used to measure the transmission efficiency of the system. An NF-5035S electromagnetic radiation analyzer is used to measure the magnetic induction intensity. The detailed physical parameters of the coils are shown in Table 2.

Table 2. Coil physical parameters table.

Parameter Name	Physical meaning	Value
L_1/μH	Self-inductance of the transmitting	283
L_2/μH	Self-inductance of the receiving coil	283
L_3, L_5/μH	Self-inductance of shielding coils 3 and 5	25.3
L_4, L_6/μH	Self-inductance of shielding coils 4 and 6	16.3
C_1/nF	Resonant capacitance of the transmitter coil	12
C_2/nF	Resonant capacitance of the receiving coil	12
C_3, C_5/nF	Shielding coil 1, 3 matching capacitors	101
C_4, C_6/nF	Shielding coil 2, 4 matching capacitors	164
R_1/mΩ	Parasitic resistance of the transmitting coil	700
R_2/mΩ	Parasitic resistance of the receiver coil	700
R_3, R_5/mΩ	Shielding coil 1, 3 parasitic resistance	40
R_4, R_6/mΩ	Shielding coil 2, 4 parasitic resistance	40
f_0/kHz	Operating frequency	85
R_L/Ω	Load	50

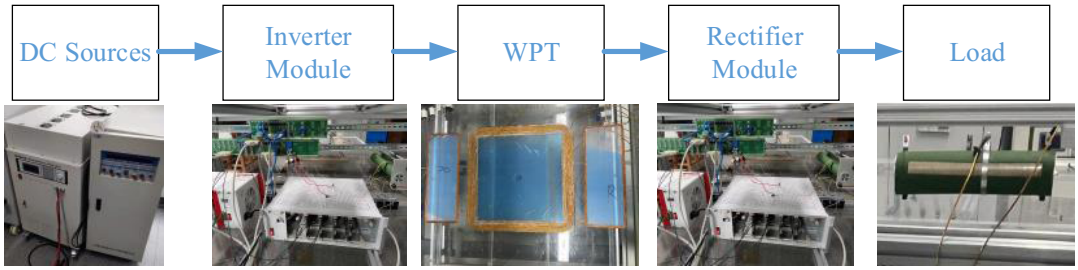

Figure 6. System framework diagram.

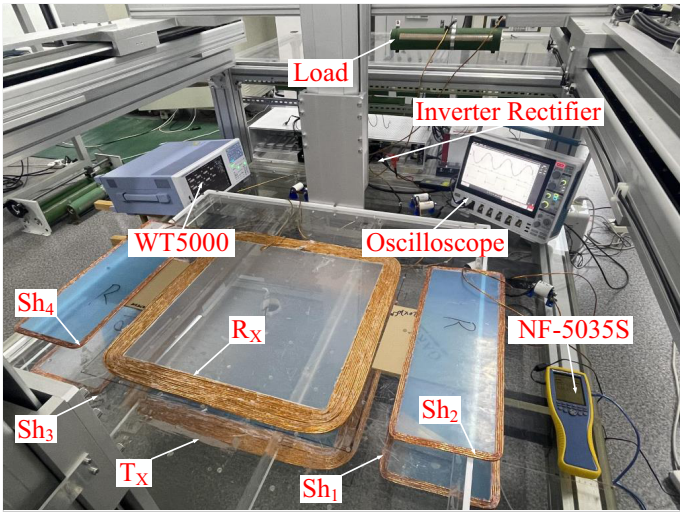

Figure 7. Experimental physical diagram.

5.2. Systematic Leakage of Magnetic Fields

To test the leakage magnetic field of the system, this subsection compares the WPT without a shielding coil system, the WPT single-layer shielding coil system, and the WPT double-layer shielding coil system.

When the system output power is 4 kW, first, MATLAB is used to calculate the distribution of the theoretical value of the leakage field B_c on the target surface and find the coordinates of the maximum leakage point. Second, the magnetic leakage B_s at the maximum leakage point is obtained using Ansys Maxwell finite element simulation software. Finally, the leakage magnetic field at this maximum leakage point is measured as B_e by using the electromagnetic radiation analyzer NF-5035S.

5.2.1. Without Shielding Coil

Figure 8 shows the distribution of the theoretical values on the observation surface for this system without a shielding coil and without offset. It can be seen that the leakage at the maximum leakage point is 14.19 μT.

Figure 9 shows the distribution of the simulation values on the observation surface for this system without a shielding coil and without offset. The simulated value of magnetic leakage at the maximum leakage point is 14.22 μT. The leakage is mainly concentrated in a local area near the transmitting coil, which is consistent with the theoretical distribution in Figure 8.

Figure 10 shows the theoretical, simulated, and measured magnitudes of the leakage at the maximum magnetic leakage point for the 0–10 cm offset cases without a shielding coil.

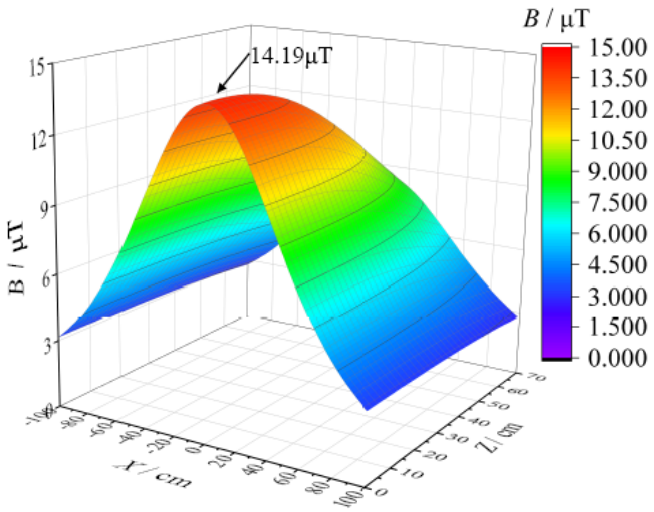

Figure 8. Distribution of the theoretical values of the magnetic leakage without a shielding coil.

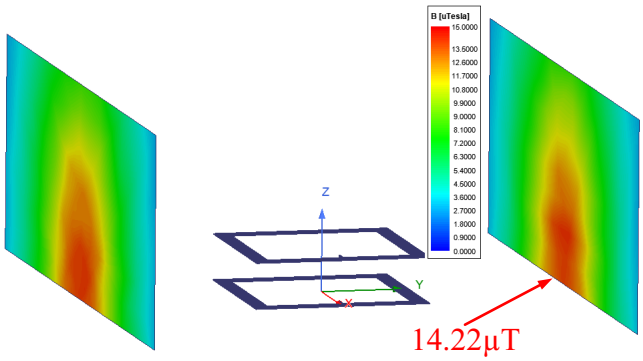

Figure 9. Distribution of the simulation values of the magnetic leakage without a shielding coil.

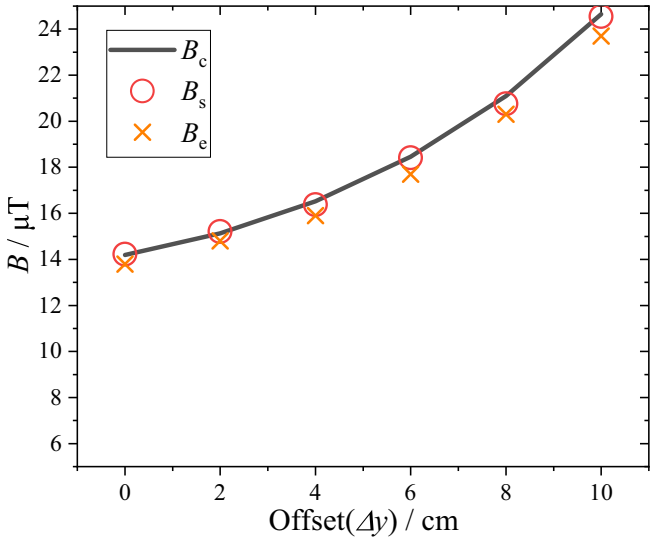

Figure 10. Maximum magnetic leakage point leakage at different offset distances without a shielding coil.

5.2.2. Single-Layer Magnetic Shielding Coils

Figure 11 shows the distribution of the theoretical values on the observation surface for the system with single-layer shielding coils without offset. It can be seen that its leakage at the maximum magnetic leakage point is 10.59 μT, and the theoretical value of the maximum magnetic leakage point is reduced by 25.37% compared to the system without a shielding coil.

Figure 12 shows the distribution of the simulated values on the observation surface for the system with single-layer shielding coils without offset. Its maximum magnetic leakage point leakage simulation value is 10.73 μT; compared to the system without a shielding coil, the maximum leakage point magnetic leakage simulation value is reduced by 24.54%, consistent with the calculated values of the theoretical distribution in Figure 11.

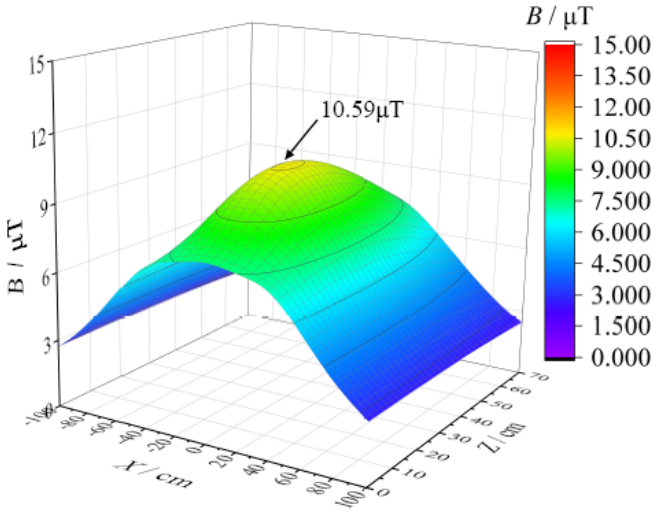

Figure 11. Distribution of the theoretical values of the magnetic leakage for single-layer shielding coils.

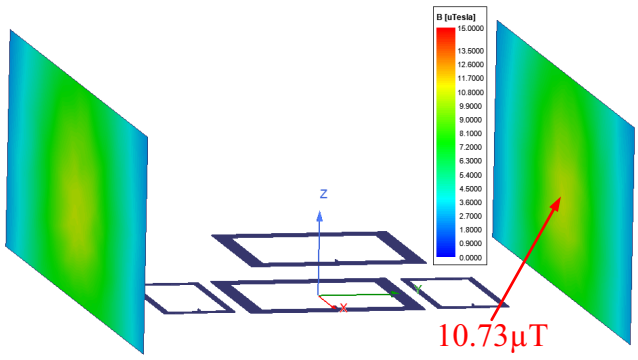

Figure 12. Distribution of the simulated values of the magnetic leakage for single-layer shielding coils.

Figure 13 shows the theoretical, simulated, and measured magnitudes of the leakage at the maximum magnetic leakage point for the 0–10 cm offset cases with single-layer shielding coils.

5.2.3. Double-Layer Magnetic Shielding Coils

Figure 14 shows the distribution of the theoretical values on the observation surface for the system with double-layer shielding coils and no offset. The maximum magnetic leakage point has a magnetic leakage of 6.46 μT. This is 54.47% lower than the theoretical value of the maximum magnetic leakage point

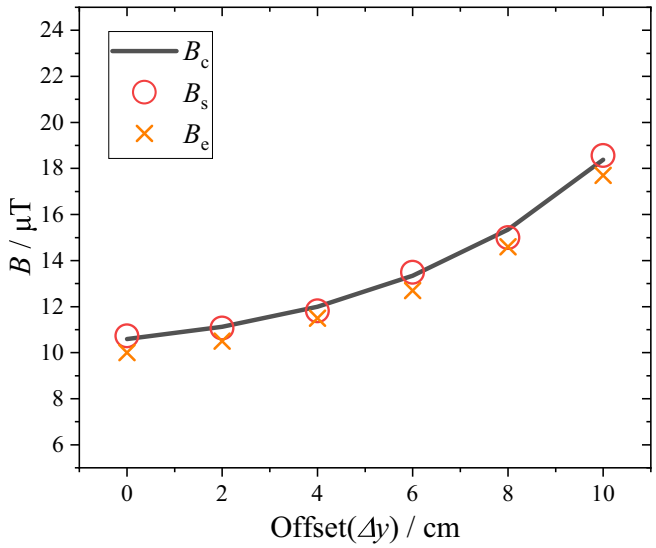

Figure 13. Maximum magnetic leakage point leakage at different offset distances in the case of single-layer shielding coils.

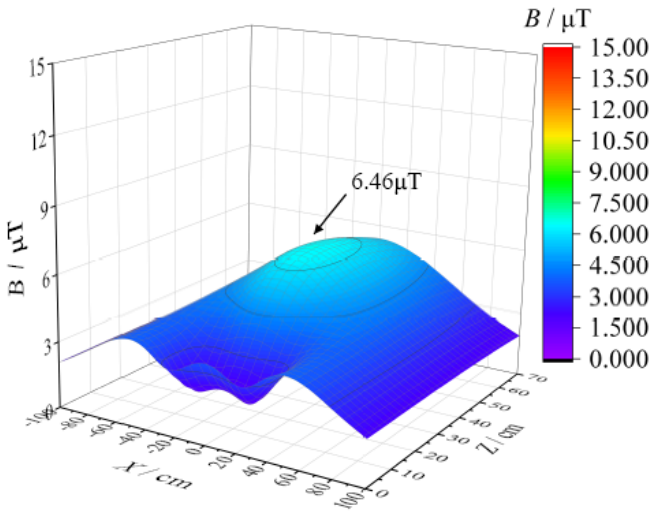

Figure 14. Distribution of the theoretical values of the magnetic leakage of double-layer shielding coils.

of the system without shielding coils. The theoretical value of the leakage at the maximum magnetic leakage point is reduced by 39% compared to the system with single-layer shielding coils.

Figure 15 shows the distribution of the simulated values on the observation surface for this system with double-layer shielding coils and no offset. The maximum magnetic leakage point has a simulated magnetic leakage value of 6.45 μT. This is 54.64% lower than the simulated leakage value at the maximum magnetic leakage point for the system without a shielding coil. The simulated leakage value at the maximum magnetic leakage point is reduced by 39.89% compared to the system with single-layer shielding coils. This is consistent with the calculated value of the theoretical distribution in Figure 14.

Figure 16 shows the theoretical, simulated, and measured magnitudes of the leakage at the maximum magnetic leakage point at 0–10 cm offsets for the double-layer shielding coils.

As seen in this subsection, the addition of the shielding coil significantly reduces the magnetic leakage, indicating that the structure has a good shielding effect.

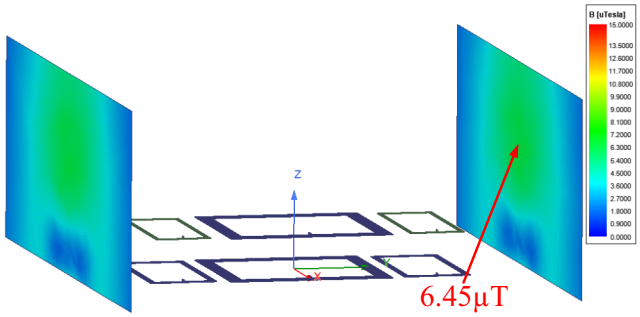

Figure 15. Distribution of the simulation values of the magnetic leakage of double-layer shielding coils.

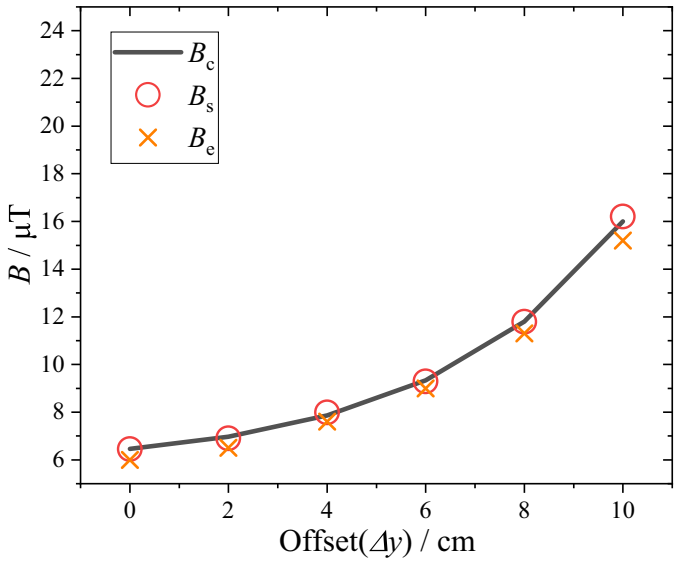

Figure 16. Leakage at the maximum leakage point for different offset distances in the case of double-layer shielding coils.

5.3. System Transmission Efficiency

To measure the change in the system transmission efficiency at 4 kW power, the theoretical value of the system transmission efficiency η_c was first obtained by calculation. Next, the simulation value η_s was obtained by MATLAB/Simulink. Finally, the measured value of the system transmission efficiency, η_e, was measured by a WT5000 power analyzer.

Figure 17 shows the efficiency of the system for different offset cases. It is shown that the system efficiency gradually decreases with increasing offset distance due to the gradual reduction of the mutual inductance between the transmitting and receiving coils caused by the offset. Furthermore, a comparison of the two groups with double-layer shielding coils and without shielding coils indicates that the double-layer structure proposed in this paper, with the addition of shielding coils, hardly interferes with the transmission efficiency.

5.4. Performance Comparison

This subsection focuses on a comparison with other studies. This comparison includes the shielding methods, shielding efficiency, and transmission efficiency. The results are shown in Table 3, which shows that the proposed structure in this paper has better shielding efficiency and transmission efficiency.

Table 3. Performance comparison table.

Documentary sources	Shielding methods	Shielding efficiency	Transmission efficiency
[22]	Without source coils	30.8%	/
[25]	Without source coils	45%	70%
[26]	Source coils	51%	92.8%
[27]	Without source coils	46.7%	92%
This paper	Without source coils	54.64%	94.8%

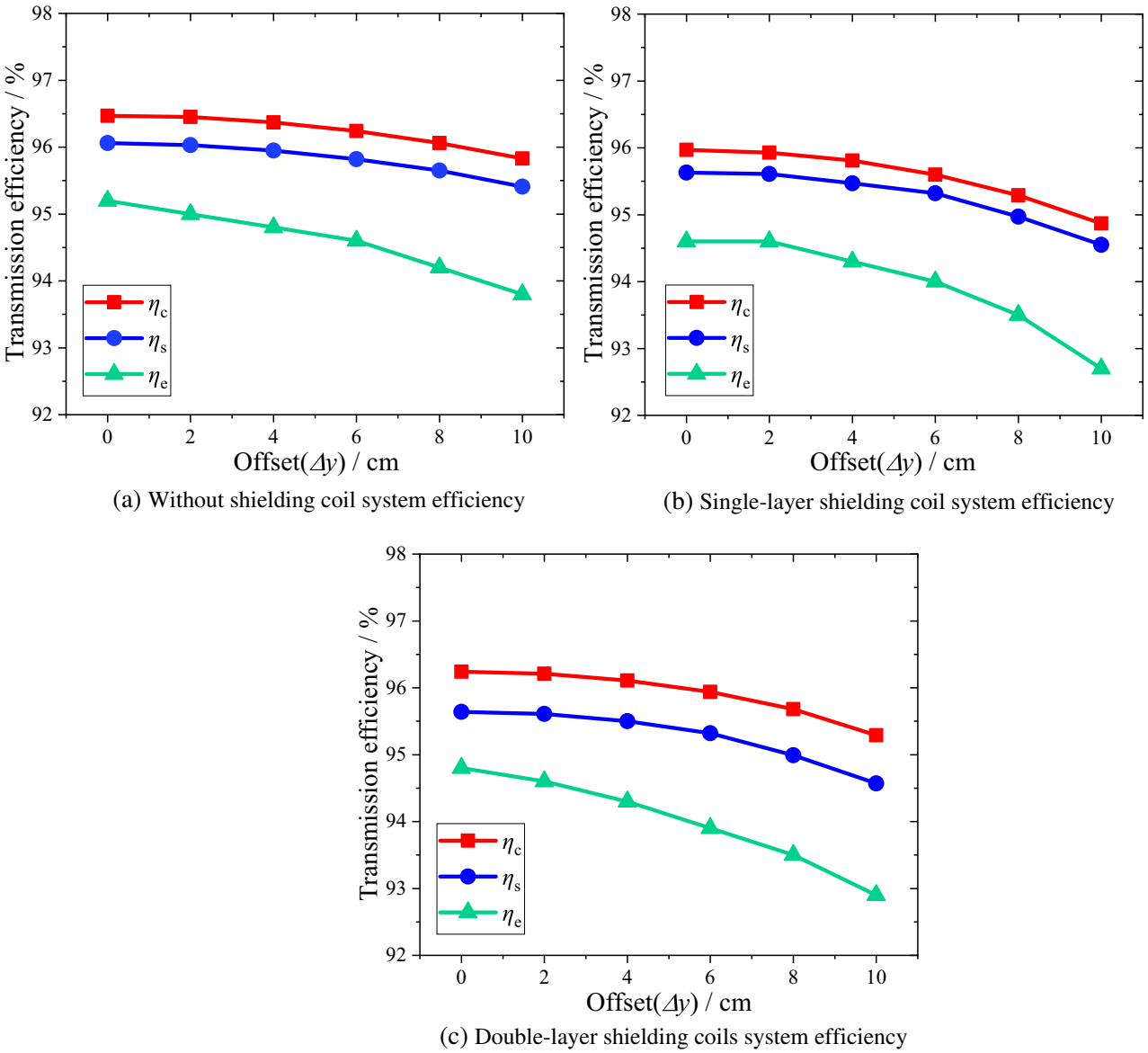

(a) Without shielding coil system efficiency

(b) Single-layer shielding coil system efficiency

(c) Double-layer shielding coils system efficiency

Figure 17. System transmission efficiency.

6. CONCLUSION

This paper proposes a WPT electromagnetic shielding structure with double-layer shielding coils for electric vehicles. The main feature of this structure is the incorporation of a double-layer of shielding coils and the use of the magnetic leakage of the WPT system to weaken the maximum magnetic leakage in the target area. The electric vehicle can be shielded when the offset is within 10 cm along the Y axis, and this feature provides a theoretical basis for the magnetic shielding structure. In addition, an optimization method of the coil parameters is proposed. Through the proposed optimization method, the optimal parameters of each shielding coil can be obtained. Then, the safe leakage magnetic field at the target power is obtained using the optimal parameters. The proposed structure is simple, and the system transmission efficiency is not affected. With 54.64% weakening of magnetic leakage, the system transmission efficiency remains above 94.8%. For static WPT of electric vehicles, both user safety and high transmission efficiency can be ensured. In the future, metallic materials should be added to further reduce magnetic leakage while improving the transmission efficiency.

ACKNOWLEDGMENT

This work was supported in part by Grant No. 2022YFB3403200 from the National Key Research and Development Program Project Fund and in part by Grant No. 2022JJ30226 from the Hunan Provincial Natural Science Foundation.

REFERENCES

1. Lu, J. and J. Zhao, "Research on electric vehicle dynamic wireless charging system with two coils in series," *Journal of Power Supply*, 1–15, Jul. 2022.
2. Rituraj, G. and P. Kumar, "A new magnetic structure of unipolar rectangular coils in WPT systems to minimize the ferrite volume while maintaining maximum coupling," *IEEE Transactions on Circuits and Systems*, Vol. 68, No. 6, 2072–2076, Jun. 2021.
3. Li, J. and J. Li, "Design and optimization of asymmetric and reverse series coil structure for obtaining quasi-constant mutual inductance in dynamic wireless charging system for electric vehicles," *IEEE Transactions on Vehicular Technology*, Vol. 71, No. 3, 2560–2572, Mar. 2021.
4. Zhang, J. and Q. Yang, "Optimization and characteristic analysis of wireless power driven vehicle featuring magnetic coupled resonance," *Transaction of China Electrotechnical Society*, Vol. 30, No. S1, 286–291, Sep. 2015.
5. Chen, J. and Z. Liu, "Research on multi coil reactive shielding of resonant wireless energy supply cardiac pacemaker," *Transaction of China Electrotechnical Society*, Vol. 37, No. 11, 2673–2685, Jun. 2022.
6. Cui, S. and B. Song, "A narrow-width three phase magnetic coupling mechanism with constant output power for electric vehicles dynamic wireless charging," *2018 IEEE PELS Workshop on Emerging Technologies-Wireless Power Transfer (WoW)*, 1–6, Jun. 2018.
7. Wang, J. and X. Wang, "Advances of wireless charging technology in electric vehicle," *Journal of Power Supply*, No. 3, 27–32, May 2014.
8. Sim, B. and S. Jeong, "A near field analytical model for EMI reduction and efficiency enhancement using an nth harmonic frequency shielding coil in a loosely coupled automotive WPT system," *IEEE Transactions on Electromagnetic Compatibility*, Vol. 63, No. 3, 935–946, Jun. 2021.
9. Campi, T. and S. Cruciani, "Magnetic field mitigation by multicoil active shielding in electric vehicles equipped with wireless power charging system," *IEEE Transactions on Electromagnetic Compatibility*, Vol. 62, No. 4, 1398–1405, Aug. 2020.
10. Campi, T. and S. Cruciani, "Numerical analysis applying the AMSL method to predict the magnetic field in an ev with a WPT system," *2018 IEEE Wireless Power Transfer Conference (WPTC)*, Montreal, QC, Canada, Feb. 2019, doi: 10.1109/WPT.2018.8639279.
11. Li, J. and X. Zhang, "Study on modelling and electromagnetic safety evaluation of the wireless power transfer system for electric vehicles," *Journal of Power Supply*, 1–14, Aug. 2021.

12. Park, J. and D. Kim, "A resonant reactive shielding for planar wireless power transfer system in smartphone application," *IEEE Transactions on Electromagnetic Compatibility*, Vol. 59, No. 2, 695–703, Apr. 2017.
13. Zhu, J. and D. Chen, "Study on the magnetic field and shielding technique for an electric vehicle oriented wireless charging system," *Transaction of China Electrotechnical Society*, Vol. 30, No. S1, 143–147, Sep. 2015.
14. Lee, J. and Y. Lim, "Effective combination of soft magnetic materials for magnetic shielding," *IEEE Transactions on Magnetics*, Vol. 48, No. 11, 4550–4553, Nov. 2012.
15. Dai, Z. and X. Zhang, "Magnetic coupling mechanism with omnidirectional magnetic shielding for wireless power transfer," *IEEE Transactions on Electromagnetic Compatibility*, 1–10, Apr. 2023, doi: 10.1109/TEMC.2023.3266089.
16. Cruciani, S. and T. Campi, "Active shielding design for a dynamic wireless power transfer system," *2020 International Symposium on Electromagnetic Compatibility-EMC EUROPE*, 1–4, Sep. 2020.
17. Meng, J. and Y. Zhang, "Research of active magnetic shielding for wireless power transfer system of electric vehicles," *Advanced Technology of Electrical Engineering and Energy*, Vol. 40, No. 4, 44–51, Apr. 2021.
18. Zhou, G., "Study on the coupling mechanism magnetic radiation suppression method for wireless power transfer system of electric vehicle," Chongqing University, Chongqing, China, 2017.
19. Xu, G., "Research on electromagnetic compatibility of N-type magnetic coupler for dynamic wireless power supply of electric vehicle," Harbin Institute of Technology, Harbin, China, 2017.
20. Xu, J. and Y. Xu, "IPT resonant reactive shielding systems with the characteristics of optimal magnetic shielding effect on the target surface," *Proceedings of the CSEE*, Vol. 39, No. 18, 5490-5498+5597, Sep. 2019.
21. Lee, J. and D. Kim, "Low leakage electromagnetic field level and high efficiency using a novel hybrid loop-array design for wireless high power transfer system," *IEEE Transactions on Industrial Electronics*, Vol. 66, No. 6, 4356–4367, Jun. 2019.
22. Kim, J. and H. Park, "Design and analysis of a resonant reactive shield for a wireless power electric vehicle," *IEEE Transactions on Microwave Theory and Techniques*, Vol. 62, No. 4, 1057–1066, Apr. 2014.
23. Moon, J. and S. Kim, "Design of a resonant reactive shield with double coils and a phase shifterfor wireless charging of electric vehicles," *IEEE Transactions on Magnetics*, Vol. 51, No. 3, 1–4, Mar. 2015.
24. Li, J. and L. Li, "Mutual inductance calculation of arbitrarily positioned rectangular coils with magnetic shielding in wireless power transfer systems," *Transaction of China Electrotechnical Society*, Vol. 37, No. 17, 4294–4305, Feb. 2022.
25. Kim, J. and S. Kong, "Coil design and shielding methods for a magnetic resonant wireless power transfer system," *Proceedings of the IEEE*, Vol. 101, No. 6, 1332–1342, Mar. 2013.
26. Mi, M. and Q. Yang, "Multi-objective active shielding coil design for wireless electric vehicle charging system," *IEEE Transactions on Magnetics*, Vol. 58, No. 2, 8700505, Feb. 2022.
27. Li, R. and Q. Yang, "Efficient shielding design and optimization of wireless power transfer system with proximity coupling," *Automation of Electric Power Systems*, Vol. 43, No. 21, 163–169, Oct. 2019.